Three-Dimensional Fully Kinetic Particle-in-Cell Model of Hall-Effect Thruster

IEPC-2011-088

Presented at the 32nd International Electric Propulsion Conference,
Wiesbaden • Germany
September 11 – 15, 2011

F. Taccogna[1] and P. Minelli[2]
Istituto di Metodologie Inorganiche e di Plasmi, Consiglio Nazionale delle Ricerche, Bari, 70126, Italy

Abstract: A realistic three-dimensional fully kinetic particle simulation of a Hall-effect thruster discharge has been attempted. The model consists of a Particle-in-Cell methodology tracking electrons, Xe^+ and Xe^{++} ions in their self-consistent electric field. A detailed secondary electron emission representation is also implemented in addition with electron-atoms volume collisions. The model is able to capture the start-up transient phase and the most relevant features of axial, radial and azimuthal behaviors of the steady-state phase detecting inverted sheaths and azimuthal fluctuations in the acceleration region. The model has the potentiality to single out the different mechanisms contributing to electron anomalous cross-field transport and to investigate on the proper incidence on it.

Nomenclature

A	=	ratio of channel cross section area simulated
B	=	magnetic field
e	=	elementary charge = 1.602189×10^{-19} C
E	=	electric field / energy
f	=	geometrical scaling factor
H	=	channel width
i	=	axial mesh index
I	=	current / ionization energy (Xe) = 1.943×10^{-18} J
I_D	=	discharge current
j	=	radial mesh index / current density
k	=	azimuthal mesh index / wave number / rate coefficient
k_B	=	Boltzmann constant = 1.380662×10^{-23}
K	=	adjustable coefficient in fluctuation-induced cross-field electron mobility
l	=	characteristic size length
L_z	=	channel length
m	=	electron mass = 9.11×10^{-31} Kg.
M	=	ion mass (Xe) = 2.18×10^{-25} Kg.
n	=	density
r	=	radial direction
r_L	=	Larmor radius
r_{in}	=	inner radius of the channel = 0.03 m
r_{out}	=	outer radius of the channel = 0.05 m
V_D	=	discharge voltage

[1] Researcher, IMIP-CNR, francesco.taccogna@ba.imip.cnr.it.
[2] Researcher, IMIP-CNR, pierpaolo.minelli@ba.imip.cnr.it.

v_d = electron azimuthal drift velocity
w = macro-particle weight
z = axial direction
α = adjustable coefficient in wall-induced cross-field electron mobility
γ = total secondary electron emission coefficient
δ = true-secondary electron emission coefficient
Δt = time step
β = Hall parameter
ε_0 = vacuum permittivity = 8.854188×10^{-12} F/m
η = back-scattered electron emission coefficient
θ = azimuthal direction
λ_D = Debye length
$\mu_\perp$ = cross-field electron mobility
ν = collisional frequency
π = pi-greek = 3.1415926536
ρ = charge density / re-diffused electron emission coefficient
σ = surface charge density / cross section
τ = inverse of collisional frequency
ϕ = electric potential
ω_p = electron plasma frequency
Ω = cyclotron frequency

I. Introduction

ONE of the most important open questions in the physics of Hall effect thrusters (HET) and in which at the moment there is still a very partial knowledge concerns the electron cross-field mobility. Classical fluid theory based on collision-induced transport, i.e. electron-neutral collisions, underestimates the cross-field transport (in particular in the acceleration region of the channel, close to the exit plane), and numerical models of the discharge usually invoke adjustable diffusion coefficients to achieve results in agreement with experiments [1]. These "ad hoc" coefficients [see α and K in eqs. (1) below] change from model to model assuming different values. Moreover, recent measurements [2] based on magnetic field turbulence have found that the effective collision frequency is sufficiently smaller than the artificial one used in fluid simulations.

The reason for this enhanced cross-field transport is nowadays identified as due to:
a) electron-wall interaction (near-wall conductivity [3]):

$$\mu_\perp = \frac{\alpha}{B^2}; \tag{1.a}$$

b) azimuthal plasma fluctuations related to axial gradient-driven instabilities (Rayleigh-type [4] or electron drift [5]):

$$\mu_\perp = \frac{K}{16B}. \tag{1.b}$$

In both cases, the kinetic description of electron subsystem is crucial. For this purpose, fully kinetic particle descriptions are suitable tools. Different two-dimensional (r-z, r-θ, θ-z) fully kinetic models have been presented in the last decade [6-8] but, in the meanwhile, it has been experimentally observed that the electron density fluctuation is not just purely azimuthal, but it also has small axial (10° along -z) and radial components (6° along r) [9] and that it propagates with a phase velocity much smaller than $\boldsymbol{v}_d = \boldsymbol{E} \times \boldsymbol{B}$ drift velocity. It therefore seems that all the three coordinates play important roles in the electron cross-field transport. Surprisingly, the only three-dimensional fully kinetic model is also one of the first models, developed by Hirakawa and Arakawa [10,11] almost fifteen years ago. However, the physical representation in their model was strongly modified by artificially reducing the ion mass ratio ratio M/m, by taking the total current as input parameter and by assuming a prescribed fixed axial electric field (thus reducing the self-consistent description to r-θ).

For such a reason, the goal of this work is to develop for the first time a full kinetic three-dimensional model of the HET channel. We first describe in Sec. 2 the numerical model. The results are presented and discussed in Sec. 3.

II. Numerical Model

The computational technique used is a standard electrostatic Particle-in-Cell/Monte Carlo Collision (PIC-MCC) model [12,13]. The simulation represents an extension of previous models [7,8] and it employs MPI standard for parallelism. Typical values for operative conditions of SPT100-type thruster [14] are reported in Tab. I.

Column length	L_z = 2.5 cm
Internal cylinder radius	r_{in} = 3.45 cm
External cylinder radius	r_{out} = 5 cm
Propellant mass flow rate	$\dot{m}$=5 mg/s
Discharge voltage	V_d = 300 V
Discharge current	I_d = 4.5 A
Max radial magnetic field	$B_{r,max}$ = 180 G

TABLE I. Operative parameters of SPT100-type thruster [14].

A. Particle-in-Cell (PIC) Module

The domain, consists of the annular channel (Fig. 1) limited axially between the anode and the exit plane (forced to be at the cathode potential) and radially between the inner and outer walls. In order to lower the computational cost we have reduced the periodicity length to A=1/4 of the entire azimuthal domain. We have checked that this does not affect the results in which we are interested. In fact, as the system is periodic in the θ direction, the length of the simulation determines the modes that are allowed to develop if they are unstable. In order to makes the simulation possible, a geometrical scaling [15] of the HET has been applied reducing the axial and radial dimension by f=10 and keeping constant all the most relevant non-dimensional parameters:

$$\frac{\lambda_{eN}}{l} = const\,; \qquad (2.a)$$

$$\frac{r_L}{l} = const\,; \qquad (2.b)$$

$$\frac{\Omega_e}{\nu_{eN}} = const\,. \qquad (2.c)$$

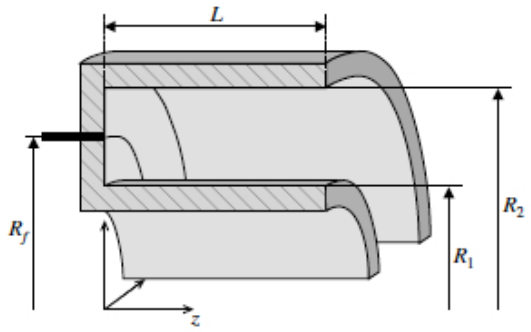

Figure 1. Sketch of the simulation domain.

In order to fulfil eqs. (2), neutral density and magnetic field have been increased by f, while the discharge current I_D has been reduced by f^2. Nevertheless, in the scaled system the ratio λ_D/H is unavoidable increased and in general the ratio between surface and volume of the channel is changed. For this reason the scaling reducing factor has been chosen such that surface effects remain controlled and still $\lambda_D << H$.

The volume of every cell is smaller than the Debye sphere. The time-step is chosen such that $\omega_p \Delta t$=0.3. Realistic values of the ion mass and vacuum permittivity have been kept.

A prescribed axial distribution (uniform in radial and azimuthal directions) of neutral density (Fig. 2.a) [16]:

$$n_{Xe}(z) = n_{Xe}(0) + 5x10^{18} \arctan\left[10\left(1 - \frac{z}{0.018}\right)\right] \qquad (3)$$

($n_{Xe}(0)$=1x10^{19} m^{-3}) and magnetic field map (Fig. 2.b) [17] (radial and axial components while B_θ=0) are imposed and fixed during the simulation (values reported corresponds to the un-scaled system). In this simulation, the temporal window investigated allows the detection of high frequency phenomena and all low frequency phenomena (so-called breathing mode) related to neutral dynamics and ionization are disregarded.

The simulation starts from an empty domain. Electrons are introduced every time step from the exit plane according to a cylindrical radial and uniform azimuthal spatial distribution and a half-Maxwellian (T_{e0}=20 eV) velocity distribution. The amount of electrons injected every PIC iteration is determined through the steady-state current control method [7]:

$$\Delta N_e = \frac{I_D \Delta t}{Aew} - \Delta N_{iC} + \Delta N_{eC} \qquad (4)$$

where $\Delta N_{i,C}$ and $\Delta N_{e,C}$ are the number of ions and electrons, respectively, passing the exit plane every PIC iteration.

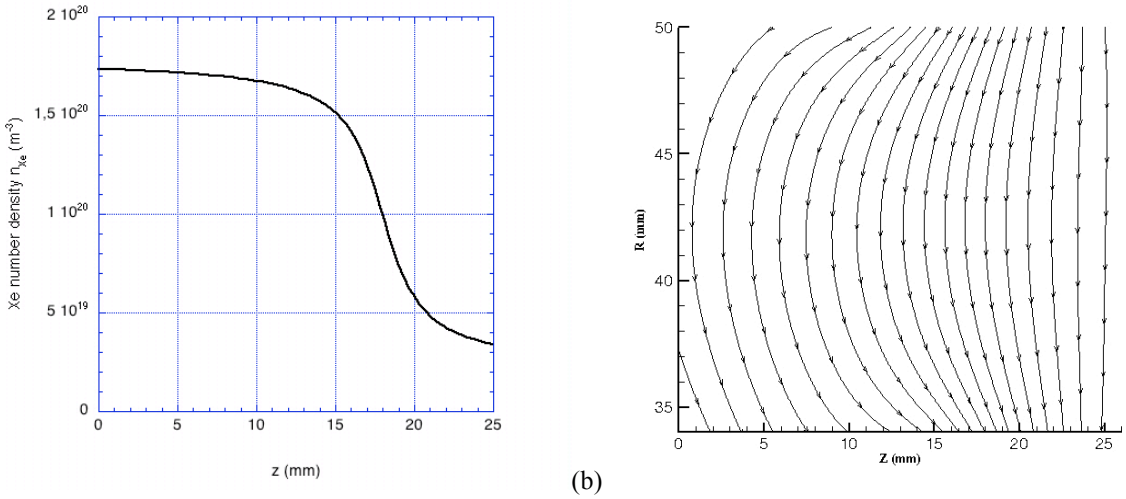

(a) (b)

Figure 2. a) Xe atoms density distribution [16] and b) magnetic field map [17] used as fixed prescribed input data in the model. All values are for un-scaled real system.

The Poisson equation in three-dimensional cylindrical geometry:

$$\left(\frac{\partial^2}{\partial r^2}+\frac{1}{r}\frac{\partial}{\partial r}+\frac{1}{r^2}\frac{\partial^2}{\partial \theta^2}+\frac{\partial^2}{\partial z^2}\right)\phi(r,\theta,z)=-\frac{\rho(r,\theta,z)}{\varepsilon_0} \tag{5.a}$$

is solved with PETSc software package [18]. For this purpose, Dirichelet fixed conditions are used on axial boarders at z=0 (anode) and at z=L_z (cathode):

$$\phi(r,\theta)\big|_{z=0}=V_D;\quad \phi(r,\theta)\big|_{z=Lz}=0, \tag{5.b}$$

while Neumann conditions are used on the insulating walls at r=r_{in} and at r=r_{out}: the electric field at the wall is normal to the surface and proportional to the net charge σ_w accumulated on the surface (the possible surface conductivity of the dielectric is neglected):

$$\left.\frac{\partial\phi(\theta,z)}{\partial r}\right|_w \overset{def}{=} -E_{r,w}(\theta,z)=\pm\frac{\sigma_w(\theta,z)}{\varepsilon_0} \tag{5.c}$$

where + is for the outer wall and – is for the inner wall. Finally, periodic boundary conditions are set on azimuthal boundaries at θ=0 and at θ=π/2

$$\phi(r,z)\big|_{\theta=0}=\phi(r,z)\big|_{\theta=\pi/2}. \tag{5.d}$$

B. Boundary Particle Module

Periodic conditions are used for particles crossing θ-boundaries. All particles (electrons and ions) are re-injected at the same radial locations and with the same velocity components from the other boundary.

When an electron hits the dielectric channel wall (BN is simulated), we choose the number of electrons emitted based on its energy E_p. It is distinguished between three different types of secondary electrons: backscattered, re-diffused and true secondary electrons. A Monte Carlo probabilistic model [19] is used which allows a detailed dependence of the secondary electron emission coefficient γ on the primary electron energy E_{p} (see Fig. 3). A lack of data is still present in the energy range below 10 eV. However, it should be pointed out that results are not very sensitive to the value of γ for E_{p}<10 eV because electrons hit the wall with low radial energy but still having enough azimuthal and axial component (the radial sheath can not have any influence on the azimuthal and axial motion, see Fig. 10 below). Concerning the angular dependence of γ, it is neglected due to the energy range considered. Finally, when an ion strikes the wall it is neutralized and deleted from the list of particles tracked.

When electrons and ions leave the simulation domain from anode and cathode planes at z=0 and z=L_z, respectively, they are deleted from the list and a counter stores the number of particles in order to compute anode and cathode currents.

C. Monte Carlo Collision (MCC) Module

We apply the standard "null collision" Monte Carlo technique [21] to simulate electron-neutral (Xe) collisions, which include elastic scattering, excitation, and single ionization.

Recently, it has also been suggested that the apparent discrepancy between classical and anomalous electron transport could be caused by an underestimation of ion current in simulations and experiment due to neglect of Xe^{++} doubly charged ions [21]. For this reason we have added collisions producing Xe^{++} ions such as direct double ionization of Xe atoms (cross section is reported in ref. [22]):

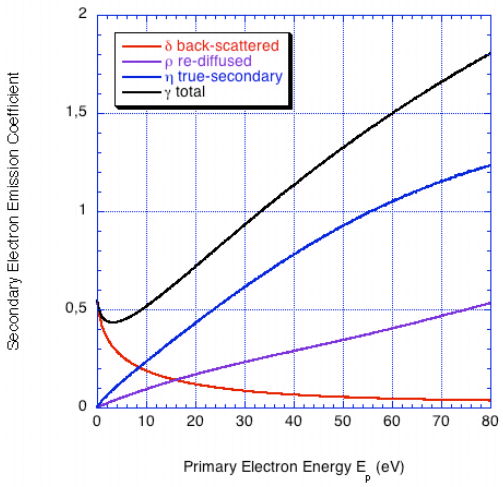

Figure 3. Secondary electron emission coefficient used in the model [19] (data correspond to BN material).

$$e + Xe \rightarrow 3e + Xe^{++} \tag{6.a}$$

and single ionization of Xe^{+} ions (cross section is reported in ref. [23]):

$$e + Xe^{+} \rightarrow 2e + Xe^{++}. \tag{6.b}$$

III. Results and Discussion

All the physical quantities shown are averaged over few tens of plasma oscillation periods. A typical run takes 9 hours on a cluster of 8 Quad Core Intel Xenon X5570 (2.93 GHz, 96 GB RAM) to reach a quasi steady-state situation with about $5x10^6$ macro-particles in the simulation domain.

A. Temporal Evolution and Start-up Transient Phase

The simulation starts from the scratch (the channel is filled by only neutrals) when the first electrons are injected from the exit plane with a rate done by I_D [see RHS of eq. (4)] (no ions are yet emitted from the exit plane). This enables us to see the ignition of the discharge.

In Figs. 4 the time evolution of a) plasma potential in the acceleration region of the channel, at z=22 mm (r=r_m and θ=θ_m), b) number of macro-particles (electron in red, Xe^{+} in blue and Xe^{++} in green) in the simulation domain, c) number of ionization events in the entire simulation domain, and d) total current (rescaled value) computed at the anode (just electron in black) and cathode (electron in red and ion Xe^{+} in blue and Xe^{++} in green), are shown as a function of the total PIC cycle (in the scaled system the time can not be easily rescaled). As we can see, three different stages can be distinguished:

a) in the first stage, the discharge is strongly electronegative, in particular, in the acceleration zone, where electrons injected are confined without reaching a sufficient energy to ionize the gas propellant; both the currents, at the anode and at the cathode are dominated by electrons; in this stage just the lateral sheath drops are formed.

b) in the second ionization stage, the ions start to be produced near the cathode (see the first peak in the number of ionization events in Fig. 4.c), but the acceleration field is not yet formed; in fact, while the electron anode current has already reached a quasi steady state value, the cathode current is still almost completely electronic.

c) in the last acceleration stage, the axial potential profile is formed and the thrust composed by the accelerated ions emitted from the exit plane is formed; the ion cathode current is composed by 90% of Xe^{+} and 10% of Xe^{++}.

This evolution agrees with images taken with a fast CCD camera [24].

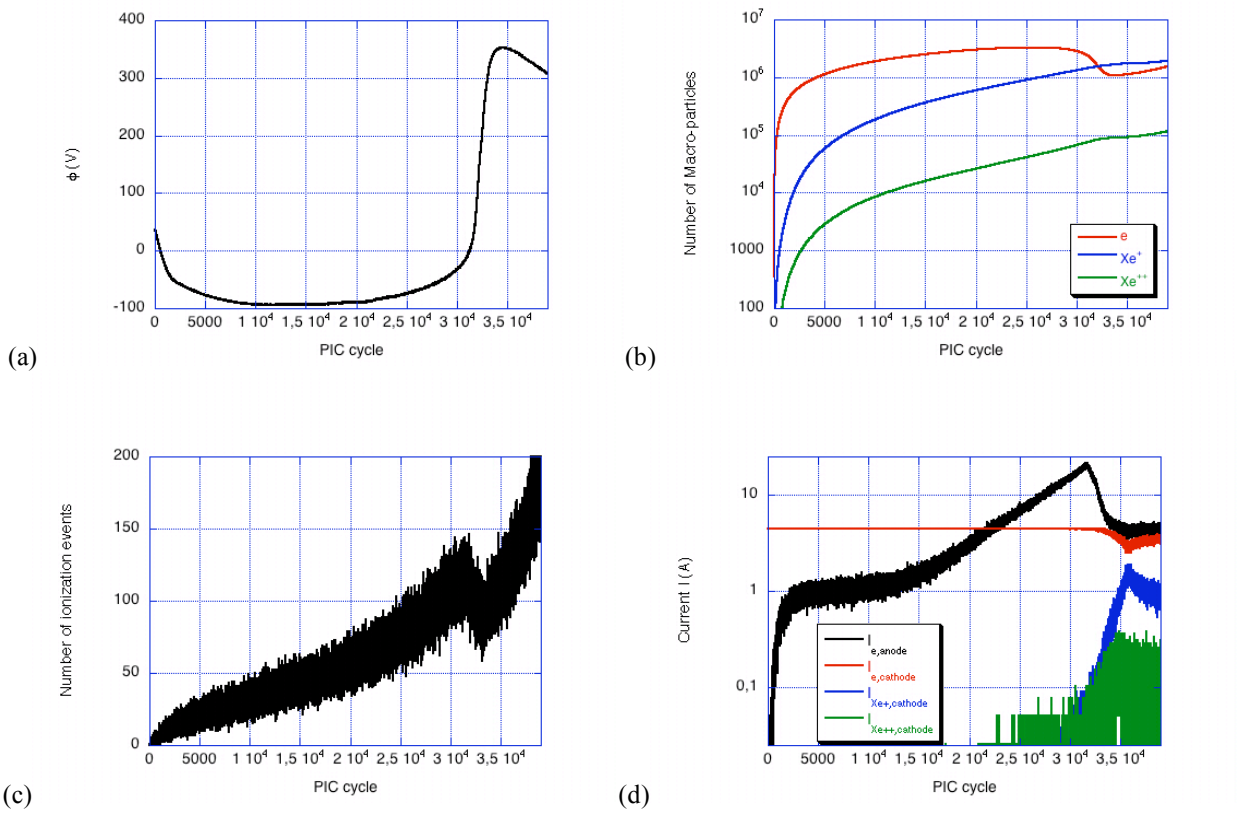

Figure 4. Temporal evolution of a) plasma potential ϕ(V) in the acceleration region of the channel, at z=22 mm (r=r_m and θ=θ_m), b) number of macro-particles (electron in red, Xe^+ in blue and Xe^{++} in green) in the simulation domain, c) number of ionization events in the simulation domain, and d) total current I(A) (rescaled value) computed at the anode (just electron, black line) and cathode (electron in red and ion, Xe^+ in blue and Xe^{++} in green), as a function of the total PIC cycle.

B. Steady-State Results

Figs. 5, 6 and 7 show electric potential ϕ(V), electron density n_e(m^{-3}) and electron temperature T_e(eV), respectively, distributions in r-z plane (at θ=θ_m), θ-z plane (at r=r_m) and r-θ plane (at z=15.65 mm). These quantities allow us to qualify and validate the model. In fact, all the most important features of the Hall discharge have been reproduced with a quantitatively agreement with previous models and measurements.

The axial distribution shows the acceleration field in the last quarter of the channel where the electron temperature reaches its maximum value of T_e=40 eV at z=15 mm.

The radial distributions (in Fig. 8.a electric potential and electron density radial profiles at z=15.65 mm and θ=θ_m have been reported) show the typical potential asymmetry and electron density peak at the walls already observed by 1D radial model [25]. Inverted sheaths are detected in the acceleration region, where secondary electron emission coefficient takes an averaged value very close to the unity. In fact, as shown in Fig. 8.b, electron energy distribution function EEDF of primary electron impacting the inner wall at z=21.875 mm is depleted just in the radial component that is the only one affected by the radial sheath. The temperature saturation mechanism does not affect azimuthal and axial components that keep the high-energy tail. This is a confirmation of the fact that in the channel it is important to distinguish between a radial $T_{e,r}$ and perpendicular to r $T_{e,\perp}$ electron temperature,

The azimuthal behaviour shows the presence of a fluctuation (see Fig. 8.c where the azimuthal profile of electric potential at z=21.875 mm and r=r_m has been reported) characterized by a wave vector $|\boldsymbol{k}|$=(12/π) rad^{-1} and directed mostly along θ.

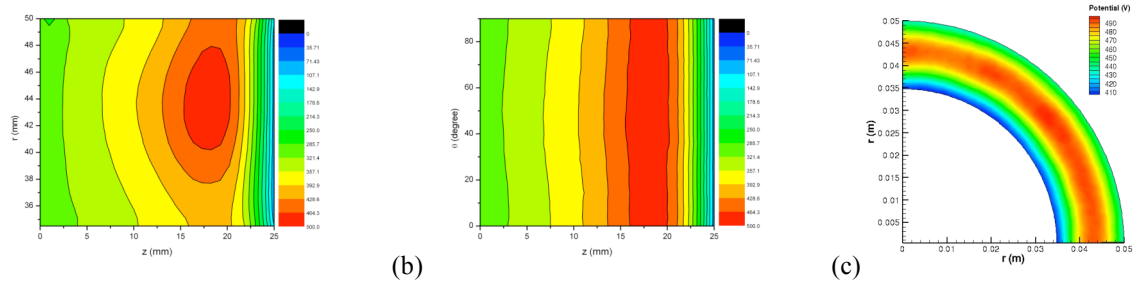

(a) (b) (c)

Figure 5. Electric potential ϕ(V) distributions in a) r-z plane (at $\theta=\theta_m$), b) θ-z plane (at $r=r_m$) and c) r-θ plane (at z=15.65 mm) at the steady state.

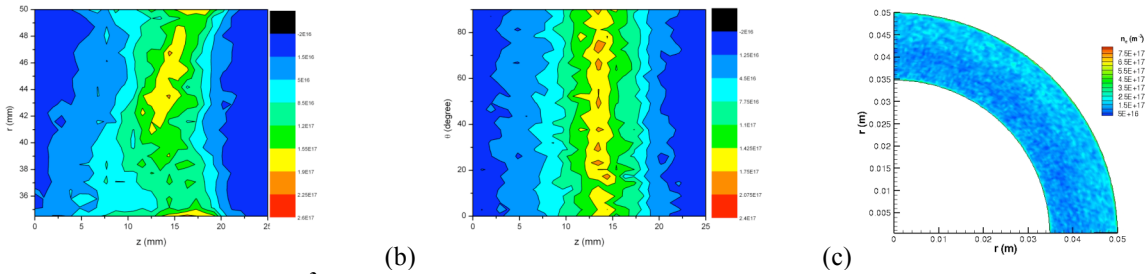

(a) (b) (c)

Figure 6. Electron density n_e(m^{-3}) distributions in a) r-z plane (at $\theta=\theta_m$), b) θ-z plane (at $r=r_m$) and c) r-θ plane (at z=15.65 mm) at the steady state.

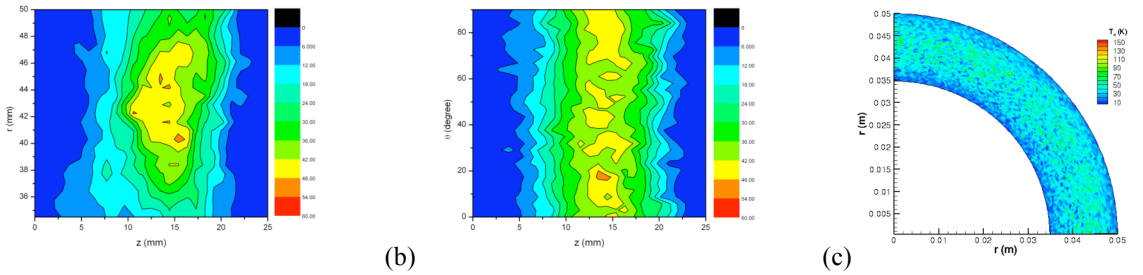

(a) (b) (c)

Figure 7. Electron temperature T_e(eV) distributions in a) r-z plane (at $\theta=\theta_m$), b) θ-z plane (at $r=r_m$) and c) r-θ plane (at z=15.65 mm) at the steady state.

IV. Conclusion

In this work a 3D fully kinetic PIC-MCC model of a Hall-effect discharge has been developed. The model includes double ionized Xe^{++} specie and a detailed secondary electron emission module using a geometrical scaling methodology. The model is able to capture all the most relevant features of the discharge: the acceleration field, inverted lateral sheaths and azimuthal fluctuations in the acceleration region of the channel. Results are quite noisy and it is necessary to reduce the macro-particle weight and increase the simulation temporal window in order to see steady state high frequency oscillations.

Furthermore, future work will concern the inclusion of part of the very-near field plume region (5 cm downstream of the exit plane) in order to realistically simulate the cathode position, include azimuthal fluctuations driven by cathode location (out of the axis) and by the negative gradient of magnetic field $\partial B/\partial z<0$ and ion reflux (recombination of ions on external thruster surface followed by re-ionization) effects.

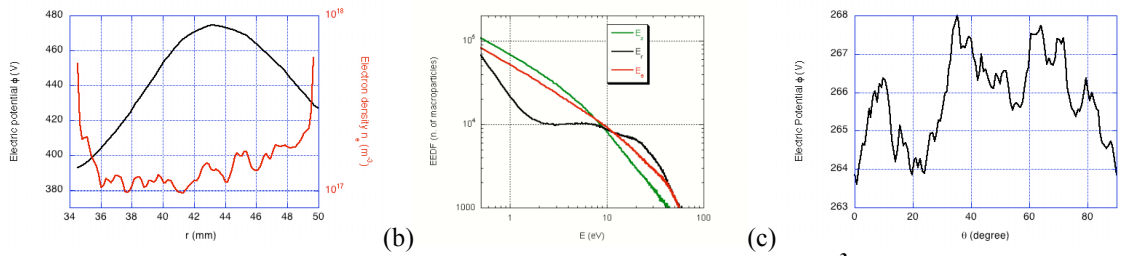

(a) (b) (c)

Figure 8. a) Radial profile of electric potential ϕ(V) and electron density n_e(m^{-3}) at z=15.65 mm and $\theta=\theta_m$. b) Energy (axial component in green, radial component in black and azimuthal component in red) distribution function EEDF of electrons hitting the inner wall at z=21.875 mm. c) Azimuthal profile of electric potential ϕ(V) at z=21.875 mm and $r=r_m$.

Acknowledgments

This work was supported by CNR Progetto di Formazione Individuale – Dipartimento Materiali e Dispositivi, fase a regime 2008/2009. Authors thank Dr. K. Matyash for B-field data.

References

[1]Meezan, N. B., Hargus, W. A. Jr., and Cappelli, M. A., "Anomalous electron mobility in a coaxial Hall discharge plasma", *Phys. Rev. E*, Vol. 63, 2001, 026410.

[2]Lazurenko, A., Dudok de Wit, T., Cavoit, C., Krasnoselskikh, V., Bouchoule, A., and Dudeck, M., "Determination of the electron anomalous mobility through measurements of turbulent magnetic field in Hall thrusters", *Phys. Plasmas,* Vol. 14, 2007, 033504.

[3]Morozov, A. I., and Savel'ev, V. V., *Reviews of Plasma Physics* Vol. 21, ed. B. B. Kadomtsev and V. D. Shafranov, New York, 2000, pp. 203.

[4]Litvak, A. A., Raitses, Y., and Fisch, N. J., "Experimental studies of high-frequency azimuthal waves in Hall thrusters" *Phys. Plasmas*, Vol. 11, No. 4, pp. 1379, 2004.

[5]Ducrocq, A., Adam, J. C., Héron, A., and Laval, G., "High-frequency electron drift instability in the cross-field configuration of Hall thrusters", *Phys. Plasmas,* Vol. 13, 102111, 2006.

[6]Adam, J. C., Héron, A., and Laval, G., "Study of stationary plasma thrusters using two-dimensional fully kinetic simulations", *Phys. Plasmas*, Vol. 11, No. 1, 2004, pp. 295-305.

[7]Taccogna, F., Longo, S., Capitelli, M., and Schneider, R., "Plasma flow in a Hall thruster," *Phys. Plasmas*, Vol. 12, 2005, 43502.

[8]Taccogna, F., Longo, S., Capitelli, M., Schneider, R., "Anomalous Transport induced by Sheath Instability in Hall Effect Thrusters", *Applied Physics Letters*, Vol. 94, 2009, 251502.

[9]Tsikata, S., Honoré, C., Lemoine, N., and Grésillon, D. M., "Three-dimensional structure of electron density fluctuations in the Hall thrusters plasma: ExB mode", *Phys. Plasmas*, Vol. 17, 2010, 112110.

[10]Hirakawa, M., and Arakawa, Y., "Particle simulation of plasma phenomena in Hall thrusters", 1995, IEPC-95-164.

[11]Hirakawa, M., and Arakawa, Y., "Numerical simulation of plasma particle behavior in a Hall thrusters", 1996, AIAA-96-3195.

[12]Eastwood, J. W., and Hockney, R. W., *Computer Simulation using Particle*, McGraw-Hill, New York, 1981.

[13]Birdsall, C. K., and Langdon, A. B., *Plasma Physics via Computer Simulation*, McGraw-Hill, New York, 1985.

[14]Bouchoule A., Cadiou A., Heron A., Dudeck M., and Lyszyk M., "An overview of the French research program on plasma thrusters for space applications", *Contrib. Plasma Phys.* Vol. 41, 2001, pp. 57.

[15]Taccogna, F., Longo, S., Capitelli, M., and Schneider, R., "Self-similarity in Hall plasma discharge. Application to particle models", *Phys. Plasmas*, Vol. 12, 2005, 053502.

[16]Garrigues, L., "Modelisation d'un Propulseur à Plasma Stationnaire pour Satellites", PhD Thesis, Universitè Paul Sabatier, Toulouse, 1998.

[17]Matyash, K., *private communication*, 2011.

[18]PETSc, Portable, Extensible Toolkit for Scientific Computation, Software Package, Vers. 3.1, Argonne Nationa Laboratory, http://www.mcs.anl.gov/petsc/petsc-as/

[19]Furman, M. A., Pivi, M. T. F., "Probabilistic model for the simulation of secondary electron emission", *Phys. Rev. Special Topics–Accel. and Beams*, Vol. 5, 2002, 124404.

[20]Vahedi, V., Surendra, M., "A Monte Carlo collision model for particle-in-cell method: applications to argon and oxygen discharges", *Comp. Phys. Comm.,* Vol. 87, 1995, pp. 179-198.

[21]Katz, I., Hofer, R., and Goebel, D., “Ion Current in Hall Thrusters", IEPC-2007-365.
[22]Jha L. K., Santosh Kumar, Roy, O. P., and Kumar, P., “Single and double ionization of Kr and Xe by electron impact”, *Phys. Scripta*, Vol. 77, 2008, 015304.
[23]Bell, E. W., Djuric, N., and Dunn, G. H., “Electron-impact ionization of In^+ and Xe^{+}”, *Phys. Rev. A*, Vol. 48, No. 6, 1993, pp. 4286-4291.
[24]Ellison, C. L., Raitses, Y., and Fish, N. J., “Fast Camera Imaging of Hall Thruster Ignition”, *IEEE Trans Plasma Sci.*, Vol. PP, Issue 99, 2011, pp. 1-2.
[25]Taccogna, F., Longo, S., Capitelli, M., and Schneider, R., "Surface-driven asymmetry and instability in the acceleration region of Hall thruster", *Contr. to Plasma Physics*, Vol. 48, No. 4, 2008, pp. 375-386.